Aerodynamic Flight-Test Results for the Adaptive Compliant Trailing Edge

Stephen B. Cumming[1], Mark S. Smith[2], Aliyah N. Ali[3], Trong T. Bui[4], and Joel C. Ellsworth[5]
NASA Armstrong Flight Research Center, Edwards, California 93523

and

Christian A. Garcia[6]
Jacobs Technology, Inc., Edwards, California 93523

The aerodynamic effects of compliant flaps installed onto a modified Gulfstream III airplane were investigated. Analyses were performed prior to flight to predict the aerodynamic effects of the flap installation. Flight tests were conducted to gather both structural and aerodynamic data. The airplane was instrumented to collect vehicle aerodynamic data and wing pressure data. A leading-edge stagnation detection system was also installed. The data from these flights were analyzed and compared with predictions. The predictive tools compared well with flight data for small flap deflections, but differences between predictions and flight estimates were greater at larger deflections. This paper describes the methods used to examine the aerodynamics data from the flight tests and provides a discussion of the flight-test results in the areas of vehicle aerodynamics, wing sectional pressure coefficient profiles, and air data.

Nomenclature

ACTE	=	Adapative Compliant Trailing Edge
BL	=	Butt Line, in.
$\bar{c}$	=	reference chord, ft
CFD	=	Computational Fluid Dynamics
C_L	=	lift coefficient
C_{L_0}	=	lift coefficient at zero angle of attack with no control deflections
$C_{L_{de}}$	=	lift coefficient derivative with respect to elevator deflection
C_{L_q}	=	lift coefficient derivative with respect to pitching moment
C_{L_α}	=	lift coefficient derivative with respect to angle of attack
C_{L_B}	=	lift coefficient bias
C_l	=	sectional lift coefficient
C_m	=	pitching moment
C_p	=	pressure coefficient
de	=	elevator position, deg

[1]Supervisory Aerospace Engineer, Aerodynamics and Propulsion Branch, P.O. Box 273 Edwards, California/MS2228, AIAA Senior Member.
[2]Aerospace Engineer, Aerodynamics and Propulsion Branch, P.O. Box 273 Edwards, California/MS2228, AIAA Senior Member.
[3]Aerospace Engineer, Aerodynamics and Propulsion Branch, P.O. Box 273 Edwards, California/MS2228, AIAA Senior Member.
[4]Aerospace Engineer, Aerodynamics and Propulsion Branch, P.O. Box 273 Edwards, California/MS2228, AIAA Senior Member.
[5]Aerospace Engineer, Aerodynamics and Propulsion Branch, P.O. Box 273 Edwards, California/MS2228, Nonmember.
[6]Aerospace Engineer, Aerodynamics and Propulsion Branch, P.O. Box 273 Edwards, California/MS2228, Member.

GIII = Gulfstream III
KCAS = Knots Calibrated Air Speed
NASA = National Aeronautics and Space Administration
p_i = Differential pressure measured at the ith pressure orifice on the left wing surface, psi
p_{ref} = Reference tank pressure, psi
p_∞ = Freestream pressure, psi
q = pitch rate, radians/sec
$\bar{q}$ = Dynamic Pressure
SCRAT = SubsoniC Research Aircraft Testbed
U_ξ = uncertainty in variable ξ
V_S = stall speed, knots
V_∞ = freestream airspeed, ft/sec
α = angle of attack, deg
ΔC_L = change in lift coefficient
ΔC_m = change in pitching moment
σ = standard deviation
$\wedge$ = estimate

I. Introduction

THE Adaptive Compliant Trailing Edge (ACTE) flap is a technology tested in support of the National Aeronautics and Space Administration (NASA) Environmentally Responsible Aviation project and developed in conjunction with the U. S. Air Force Research Laboratory (Wright Patterson Air Force Base, Ohio). The flap consists of a rigid center section that connects to the wing on each side via a transition section, eliminating gaps that produce acoustic noise and reduce aerodynamic efficiency. The technology also has potential to allow for weight savings in future aircraft.

To demonstrate the ACTE flap technology, the NASA Armstrong Flight Research Center (Edwards, California) testbed Gulfstream III (GIII) airplane (Gulfstream Aerospace Corporation, Savannah, Georgia) was modified. The GIII standard Fowler flaps were removed and replaced with ACTE flaps. The flaps were fixed to specific deflections prior to flight and were only adjustable on the ground. The airplane was instrumented to gather vehicle aerodynamic data as well as data specifically describing the flow over the wings. The left wing was instrumented for chordwise surface pressure at three butt line locations. Butt line is used to describe locations left and right of the airplane plane of symmetry, which is located at a butt line of 0. Tufts were installed on the modified flap. A leading-edge stagnation sensing system was installed near the middle butt line location on the left wing.

The aerodynamic effects of the ACTE modification on the GIII airplane were predicted through Navier-Stokes computational fluid dynamics (CFD) simulations. A model of the aerodynamic forces and moments generated by the ACTE flaps was created from the CFD results and was used for safety of flight studies and flight planning. The CFD results were also used to predict changes to airflow over the wing at discreet sectional locations. Additional CFD work was performed specifically to examine the ACTE modification effect on stall speed[1] and roll control.

A series of flights was flown at the NASA Armstrong Flight Research Center to obtain aerodynamic and structural data for the modified GIII airplane and the ACTE flaps. This paper will discuss the results of the flight tests, concentrating on flight-derived pressure distributions and aerodynamic force and moment estimates, and how these results compare with the pre-flight predictions along with evaluating the effectiveness of the leading-edge stagnation sensing system.

II. Vehicle Description

The ACTE flap modification was incorporated onto the NASA SubsoniC Research Aircraft Testbed (SCRAT) airplane, a GIII airplane built by Gulfstream Aerospace Corporation and equipped with instrumentation for performing flight research.[2] SCRAT can be seen with the ACTE modification installed in Fig. 1 and a three-view illustration of the airplane is shown in Fig. 2. The baseline GIII airplane uses Fowler flaps as high-lift devices. For this project, the Fowler flaps were removed and replaced with the ACTE flaps. This modification necessitated the removal of the GIII flight and ground spoilers, thereby reducing the roll control authority of the airplane. The GIII airplane has a wing area of 934.6 ft^2 and a reference span of 75 ft (which does not include the winglets). The mean aerodynamic chord is 13.78 ft. The SCRAT is powered by two Rolls-Royce Spey RB.163 Mk 511-8 turbofan engines (Rolls Royce Group

PLC, London, England), which are each capable of providing a maximum continuous thrust of 10,940 lb at sea level. Thrust reversers are fitted to each engine to reduce landing distance. The service ceiling of the SCRAT is 45,000 ft MSL, and the maximum velocity is 340 knots calibrated air speed and a maximum Mach number of 0.85. For the purposes of the ACTE flight test, the maximum Mach number was limited to 0.75 and the maximum altitude was limited to 40,000 ft MSL. The SCRAT has an empty weight of approximately 38,000 lb and a maximum takeoff weight of 69,700 lb.

Extensive flight research instrumentation was added to the plane. Much of the research instrumentation was for structural measurements on the wings (e.g., strain gauges, accelerometers, and fiber optic strain sensing).[3,4] The wings were also equipped with pressure sensors to measure both steady and unsteady pressures. For flight mechanics measurements, an embedded global positioning system (GPS)/inertial navigation system (INS) was installed and served as the primary source of angular rate, linear acceleration, and Euler angle measurements. Four flow angle vanes were mounted on the top part of the nose of the airplane, from which angles of attack and sideslip were calculated. Pressure transducers were installed in the pitot and static pressure lines of the production pitot-static system so that airspeed and altitude could be calculated. Control surface position measurement devices were installed on all surfaces. The airplane was not equipped for thrust measurements, though the power lever angle and other engine parameters were measured. Fuel weights were radioed by the aircrew to the control room at the end of each flight card. These weights were tabulated and interpolated with time during data processing to provide fuel weight estimates that were used, along ground measurements taken prior to each flight series, to determine gross weight, center of gravity, and moments of inertia.

An illustration of an ACTE flap is shown in Fig. 3. The ACTE flaps were designed and built by FlexSys, Inc. (Ann Arbor, Michigan). Each flap consists of a rigid center section and two end sections. The end sections are referred to as transition sections, as they form the transition between the rigid part of the flap and the traditional wing structure. The overall spanwise length of each flap is 18 ft. The flaps are roughly 20 percent of the wing chord. The flight-test deflection range was from -2 deg (trailing edge up) to 30 deg (trailing edge down). They were designed so that the 0-deg flap deflections of the fowler flaps and ACTE flaps would have nearly identical shapes.

The ACTE flaps were positioned on the ground prior to each flight and were not capable of in-flight acutation. After being positioned, the flaps were imaged using a laser scanner to verify they met surface accuracy requirements. These requirements included left-right symmetry and reasonable matching with the geometry of the models used for pre-flight aerodynamic analysis. After flight, they were rescanned, to determine if the outer mold line of either flap had changed due to aerodynamic loads.

To collect airflow data over the modified wing, pressure sensors were installed at three butt line locations (BL 136, BL 201, and BL 269) on the left wing of the airplane. Other aerodynamic sensors, including the leading-edge stagnation detection system and tufts, were installed in close proximity to the center butt line (BL 201) to obtain additional data. Two types of tufts were installed on the wing. One set of tufts located just inboard of the pressure sensors at BL 201 were separation detection sensors developed by Rolling Hills Research Corporation (El Segundo, California) that were connected to the flight instrumentation system and provided digital estimates of separated and attached flow for each tuft. The other tufts located further inboard were constructed from parachute cord and qualitatively analyzed via video. Figure 4 illustrates the general layout of the aerodynamic sensors on the left wing. The test airplane was equipped with cameras mounted externally on the fuselage that provided views of the ACTE flaps and were telemetered to the control room during flight.

The pressure sensors installed at each of the three butt lines consisted of both flush- and surface-mounted pressures. To measure steady pressures, pressure taps were drilled into the leading edge and vinyl tubing with drilled holes was applied over the rest of the wing. The pressures for each port were measured by electronic differential pressure scanners with a +/-15 lb/in^2 differential pressure range. Two of these units were installed in the leading edge of the wing, and one was located in the flap cove area. The two electronic differential pressure scanners in the leading edge were connected to a single reference volume with pressure measured by a pressure transducer with a 0-15 lb/in^2 absolute pressure range. The single electronic differential pressure scanner in the flap cove area was connected to a reference volume that had pressure measured by a miniature pressure transducer with a 0-15 lb/in^2 absolute range. Near each of the three pressure lines on the aft portion of the wing and the flap were surface mounted absolute pressure transducers, capturing data at 1,000 samples per second. These pressure transducers were installed to capture any unsteady pressure events over the aft portion of the wing and flap.

III. Flight-Test Approach

In preparation for the ACTE flights, two series of flights with the baseline GIII airplane were flown, and aerodynamic analyses were performed. Following installation of the ACTE flaps on the GIII airplane, a series of flights were flown with the ACTE flap in various configurations.

A. Baseline Flights

Prior to flying the GIII airplane with the ACTE flaps installed, two series of flights were completed with the baseline GIII airplane. The first series consisted of nine flights and was flown with the GIII airplane in a standard configuration. The second series of flights consisted of five flights and several of the flights were flown with the flight spoilers disabled in order to evaluate roll control without those surfaces operating. Both series of flights served to collect aerodynamic and structural data for the unmodified GIII airplane. Data from these flights were used to update existing aerodynamic models for the GIII airplane and gather other baseline aerodynamic data for the airplane, including calibrations for both flow measurement and pitot-static systems and wing pressures.

B. Pre-Flight Analyses for ACTE Configuration

Pre-flight analysis for the ACTE configuration consisted of CFD analyses and aerodynamic modeling of the ACTE flap. Results from the CFD analyses were used not only for the aerodynamic modeling, but also to identify potential areas of concern for flight test.

1. CFD Analyses

The aerodynamic effects of the ACTE modification on the GIII airplane were predicted through Navier-Stokes CFD. The CFD analyses were performed not only for the purpose of creating an ACTE aerodynamic model, but also for investigating effects of the flaps on stall speed, potential loss of aileron effectiveness, and for predicting pressure profiles for comparison to flight data. Analyses were also performed to predict the effects of losing the ACTE flaps transition sections to evaluate potential failure scenarios. The CFD work was done predominantly with the unstructured-grid Navier-Stokes code STAR-CCM+ (CD-Adapco, Melville, New York), in conjunction with the structured-grid code OVERFLOW.

An example of a STAR-CCM+ surface mesh for the GIII airplane with ACTE flaps is shown in Fig. 5. The full airplane was generally modeled to examine the effects of flows with sideslips on the airplane aerodynamics. The ACTE GIII airplane computer-aided design (CAD) geometry was built from two different sources. The baseline GIII airplane laser scan obtained at NASA Armstrong was combined with the ACTE flap CAD obtained from Flexys Inc. to provide the final ACTE GIII airplane CAD used in the current CFD analysis effort. Operating airplane engines were modeled in the CFD computations using engine flow conditions obtained from a 1-D engine cycle model. Unstructured polyhedral meshes were used together with prism layers to model the near-wall boundary layer flows. Nineteen prism layers are used in the near-wall region and clustered using the hyperbolic tangent stretching function. A total prism layer thickness of 1.8 in. was found to provide appropriate coverage for the boundary layer region over the wings and fuselage of the airplane. The next-to-the-wall prism layer spacing of 0.04 in. provides an average near-wall y+ value of approximately 100 over most of the solid wall surfaces on the airplane wings, fuselage, and tails. Typically about 35 million finite volume cells are used. It was found from in-house grid independence studies that this mesh size is generally sufficient to provide grid-independent solutions for the various overall airplane aerodynamic coefficients. The SST K-Omega two-equation turbulence model was used with an all-y+ wall treatment. With this treatment, turbulence wall function is automatically used when the near-wall y+ wall spacing exceeds the range of applicability of the low-y+ integrating to the wall approach. Second-order Roe flux difference splitting (FDS) was used with a coupled implicit flow solver. The full Navier-Stokes solutions are generally not considered to be limited to any speed, angle of attack, or flap deflection range, but there are uncertainties in modeling turbulence and separated flows over the ACTE flap areas.

2. Aerodynamic Modeling

A model of the aerodynamic force and moment effects of the ACTE flaps was created before the flight tests and incorporated into a six-degree-of-freedom simulation, to support readiness reviews and pilot training. The ACTE aerodynamic model was made in the form of force and moment coefficient deltas that are added to the baseline GIII aerodynamic model. The baseline model was built mostly from data from a series of flights with the unmodified GIII airplane. Pieces of the baseline model that could not be derived from flight data were filled in with parts from a previous aerodynamic model. Modeling efforts assumed that the 0-deg ACTE configuration was the same as a baseline GIII airplane.

To make the best use of schedule and resources, the complexity of the ACTE aerodynamic model increased with time, as did the complexity of the tools used to make the model. The initial model was created from empirical data and predictions from a vortex lattice code and contained only a limited number of terms. The final preflight model was based on the Navier-Stokes CFD results and included additional components, such as predictions of aerodynamic changes due to missing ACTE transition sections. This paper only presents results from the final model. Additional information about the aerodynamic modeling for the ACTE project can be found in Ref. 5.

C. ACTE Flights

A series of 23 flights were flown to clear the ACTE flight envelope and collect research data for the full range of ACTE flight-test deflections. The flight envelope for each flight was dependent on the ACTE deflection. Figure 6 shows the flight envelopes for the different ACTE deflections along with all aerodynamic test points flown during the flight series.

As a means of managing risk, the first flights with the ACTE flap installed were at 0 deg. At this deflection, the outer mold line of the modified GIII airplane was nearly unchanged from a baseline GIII airplane. Once the 0-deg flight envelope was cleared, the ACTE flap deflection was changed to 2 deg for another set of flights. The ACTE flap deflection was increased incrementally to a maximum of 30 deg. A deflection of -2 deg (trailing edge up) was also flown. Table 1 lists all deflections flown, in order of envelope expansion, along with the total number of flights at each deflection.

Table 1. ACTE flight series breakdown.

ACTE flap deflection (deg)	Number of flights
0	4
2	3
5	4
10	1
12.5	1
15	1
17.5	1
20	1
25	1
-2	4
30	1

During each flight, various maneuvers were flown to collect structural, handling qualities, and aerodynamic data. This paper will discuss maneuvers flown to collect aerodynamic data. Additional information on structural maneuvers and data collected can be found in Refs. 3 and 4. The aerodynamic areas of interest included vehicle aerodynamics, airflow over the modified wing, and potential effects on the pitot-static system. Maneuvers were flown throughout the flight envelope at each ACTE deflection to gather aerodynamic data in these areas. Pitch and yaw/roll parameter estimation maneuvers were performed in sets of three to evaluate vehicle aerodynamics. Thirty-second steady state points (constant airspeed and constant altitude) were flown to capture steady-state airflow over the modified wing. Constant pressure altitude accelerations and constant pressure altitude decelerations were flown to capture data for pitot-static system evaluation.

IV. Investigation Methods

A. Vehicle Aerodynamics

Vehicle aerodynamics were estimated using standard aircraft stability and control parameter estimation methods, namely equation error[6] and output error[7] techniques. Both techniques produced similar results for this work. The results presented in this paper are from output error. Of primary interest for this work were the effects of the ACTE

flaps on the test airplane lift and pitching moment. Since thrust was not measured, drag effects could not be accurately computed.

The lift coefficient, C_L , was modeled as Eq. (1):

$$C_L = C_{L_B} + C_{L_\alpha}\alpha + C_{L_q}\frac{q\bar{c}}{2V_\infty} + C_{L_{de}}de \tag{1}$$

Pitching moment coefficient used the same model setup. The term, C_{L_B}, is a bias term that is different than the airplane zero angle-of-attack lift, C_{L_0}, because it comes from the linearization of the aerodynamics and contains the aerodynamic contributions of the deflected stabilizer, elevator tab, and ACTE flaps. The bias term can also collect the effects of measurement biases. The estimated pitching moment bias term had to be adjusted for elevator tab effects because the tab position was not the same for every maneuver, and elevator tab derivatives were not identifiable from the flight data. Tab contributions were removed from the bias term estimates using values from the baseline GIII aerodynamic model. The stabilizer contributions to lift and pitching moment were not removed, since all configurations used the same stabilizer position.

The lift coefficient increment due to ACTE flaps, ΔC_L , was calculated from the parameter estimation results using Eq. (2):

$$\Delta C_L = \hat{C}_{L_{B,2}} - \hat{C}_{L_{B,1}} + \alpha_2\left(\hat{C}_{L_{\alpha,2}} - \hat{C}_{L_{\alpha,1}}\right) \tag{2}$$

where "2" denotes the deflected ACTE estimates and "1" denotes the estimates for the undeflected ACTE flap. This ΔC_L amounts to the difference between the lift of the GIII airplane with deflected ACTE flaps at trim and the predicted lift of the GIII airplane with undeflected ACTE flaps at that trim angle of attack. The pitching moment change was computed the same way. Parameter estimation maneuvers were typically flown in sets of three. Parameter estimates from the three maneuvers at each test point were blended into a weighted mean based on their individual standard errors to reduce the number of points for presentation. Overall confidence bounds were computed using estimated standard errors for the weighted means and ordinary uncertainty analysis calculations[8] shown in Eq. (3):

$$U^2_{\Delta C_L} = \hat{\sigma}^2_{\hat{C}_{L_{B,2}}} + \hat{\sigma}^2_{\hat{C}_{L_{B,1}}} + \alpha_2^2\left(\hat{\sigma}^2_{\hat{C}_{L_{\alpha,2}}} + \hat{\sigma}^2_{\hat{C}_{L_{\alpha,1}}}\right) \tag{3}$$

The calculation in Eq. (3) does not take into account uncertainties in the angle-of-attack measurement or in the lift coefficient itself. It also does not take into account the covariance term for $\hat{C}_{L_B}$ and $\hat{C}_{L_\alpha}$, which is typically negative and would serve to reduce the uncertainties.

B. Sectional Pressures

Pressure data were collected from the previously discussed steady pressure ports at BL 136, BL 201, and BL 269. These pressure data were used to calculate the C_p distribution across the three butt lines.

Due to the inherent pneumatic lag in the pressure measurements, the pressure data were only useful for steady state maneuvers. Steady state maneuvers were targeted to last approximately 30 seconds, although these maneuvers often lasted 1 to 2 minutes during the flight test in order to capture sufficient data. This data were reviewed to find a 5-second span of time where there was minimal change in Mach, altitude, and angle of attack; and then the data were averaged over this 5-second time span. The pressure coefficient at the ith port, C_{pi} , was calculated with the averaged values of the pressure at the port; p_i, the pressure of the reference tank associated with that pressure scanner; p_{ref}, freestream pressure; $p_{\infty,}$ and dynamic pressure; $\bar{q}$. The C_p calculation is provided in Eq. (4):

$$C_p = \frac{p_i + p_{ref} - p_\infty}{\bar{q}} \tag{4}$$

C. Stagnation Point Estimation

A sensor was installed to track the leading-edge stagnation point throughout the ACTE flights to provide additional insight into flow over the wing. The leading edge stagnation point sensor is comprised of a 32-element Senflex® hot-film array[9] (Tao of Systems Integration, Inc., Hampton, Virginia) and its associated electronics box. The electronics box is self-calibrating at startup and outputs values proportional to voltage and current for each sensor element. These

values are then easily converted to power consumption for each sensor. Since power consumption is proportional to shear stress on surface mounted hot films, the sensor with the least power consumption should be the location of the stagnation point.

D. Air Data

The production GIII pitot-static system was found to be affected by the position of the standard GIII Fowler flap during baseline flights, resulting in a discrepancy of up to approximately Mach 0.007, so the effects of the ACTE flaps on the system were of interest. The GIII production pitot-static system consists of total pressure probes mounted on the nose of the airplane and flush static ports on the both sides of the fuselage, approximately 10 ft forward of the wing. The production pitot-static system was checked throughout the ACTE flight phase through a series of constant pressure altitude accelerations and constant pressure altitude decelerations. The accelerations and decelerations were performed at multiple altitudes for various Mach number ranges. The acceleration maneuvers included tower flybys flown approximately 200 ft above the ground past an instrumented tower. These flybys provided more accurate calibration data than maneuvers at higher altitudes due to the proximity to the tower sensors, the ability to get meteorological measurements at one-minute intervals, and the accuracy of the tower sensors. Meteorological data from sounding balloons and tower instrumentation were used to calculate free stream static pressure at the airplane flight altitude, which was provided by a differential GPS. This true static pressure was used along with data from the production pitot-static system to create static-position error correction curves, using the methodology given in Ref. 10.

V. Flight-Test Results

As previously discussed, a total of 23 flights were flown with the ACTE flap installed. Substantial aerodynamic data were collected during these flights and subsequently analyzed. Results are discussed for vehicle aerodynamics, sectional pressures, stagnation point estimation, and air data.

A. Vehicle Aerodynamics

Other than the lift and pitching moment terms, the ACTE flaps were not found to have a significant effect on the stability and control derivatives of the test airplane. Recall that drag effects could not accurately be calculated, since thrust was not measured. Figure 7 shows the ΔC_L due to the ACTE flaps, compared to the preflight ACTE aerodynamic model that was created from CFD data. The aerodynamic model data are shown as a shaded area that represents a 95% confidence region, based on the model uncertainties. For the flight data, each symbol represents a specific flight condition for that ACTE deflection. Figure 7 shows that the model over-predicted the ΔC_L, particularly as ACTE deflection got larger. The ΔC_m results are shown in Fig. 8. Again, the aerodynamic model predicted much stronger flap effects than were found in the flight data. Figures 9 and 10 show ΔC_L and ΔC_m changes as a function of Mach number for all primary ACTE deflections. For ΔC_L, at ACTE deflections of 15 deg and below, the flight results tend to skirt along the edges of the aerodynamic model confidence regions as Mach number increases. In general, it appears that the aerodynamic model predicted stronger Mach effects on ΔC_L. For ΔC_m, the flight results track the aerodynamic model regions very well for deflections of -2, 2, and 5 deg. For deflections of 10 and 15 deg, the aerodynamic model predicted Mach trends different than those shown in the flight results, but the flight results were still within the aerodynamic model uncertainties. The ΔC_m estimates at Mach 0.35 were poor, due to the 0-deg ACTE results at that speed at 20,000-ft MSL altitude, which did not agree with other data. The values shown in Fig. 10 were created using baseline GIII flight data for that flight condition.

B. Sectional Pressures

During flight test, the pressure sensor that measured reference pressure in the flap cove reported inconsistent data. All of the steady pressure ports beyond 70% of the chord length at each of the three BL stations used this reference pressure. To correct for this issue, all of the steady pressure measurements beyond 70% chord were referenced to the pressure sensor in the wing leading edge. Given the similarity of the trends between the corrected flight data and available CFD estimates, the correction is a reasonable correction. In all of the figures illustrating pressure coefficient in this paper, a black vertical line is added to demarcate the location beyond which the reference pressure correction was made, starting with Fig. 11.

The ACTE flaps generally affected pressure profiles as expected. Pre-flight CFD predictions proved to be more accurate at lower deflections (less than 15 deg). Flow separation was under-predicted for large deflections (above 20 deg), which corroborates the differences between the CFD-predicted and flight-derived ΔC_L and ΔC_m results since less separation over the aft portion of the wing leads to higher lift and pitching moment for the predicted results.

For most flight conditions, predicted pressures on the lower surface of the wing matched well with flight data, however, the suction on the upper surface was over predicted. Figure 11 illustrates an example of this over-prediction. This discrepancy contributed to predictions of overall higher sectional and therefore, total airplane lift by the CFD data than the flight data.

As Mach and Reynolds number increased and the thickness of the boundary layer near the leading edge decreased, a difference in C_p between the flight and CFD data can be seen for the port located at x/c ≈ 0.05. An illustration of this discrepancy can be found in Fig. 12. It was found that the vinyl tubing that began between this port and the next port (at an x/c of 0.121) had a thickness that was roughly 30% of the thickness of the boundary layer at higher speeds, according to CFD data, and substantially affected this pressure tap, which was drilled into the surface of the leading edge. For reference, the Reynolds number per unit length for this flight condition was approximately 2.17 x 10^6 per foot, while it was approximately 1.61 x 10^6 per foot for the flight condition in Fig. 11, which did not show this discrepancy.

As mentioned before, separation was under-predicted by the CFD for ACTE flap deflections greater than 20 deg. Flow separation on the flap upper surface often occurs at higher ACTE flap deflections. The location of the start of the flow separation can be indicated by a sudden jump in the surface pressure distribution. For example, in Fig. 13 such a surface pressure jump is observed at the location x/c = 0.9. It can be seen here that the CFD pressure jump takes place slightly downstream of the flight data indicating smaller flow separation region than the flight data pressure distribution indicates. This behavior, with the CFD predicting full separation 4 to 6 inches aft of the flight data, was consistent for all test points with a deflection greater than 20 deg and was seen in both the pressure data and qualitatively from video of the tufts. Also, it was noted that as one moves away from the fuselage, the degree to which the CFD under-predicted flow separation near the flap increased. Figure 14 provides an example of this trend. In addition to the under-prediction of flow separation, the CFD solutions also over-predicted the suction on the upper surface of the flap prior to flow separation. This over-prediction can be seen for ports aft of x/c = 0.7 in Figs. 12, 13 and 14, with the over-prediction often increasing downstream of this location until flow separation.

Sectional lift coefficient, C_l, was estimated through the integration of the pressures along each butt line location. C_l resulting from a subset of flight and CFD data is presented in Fig. 15 and Fig. 16. The freestream conditions for this data are summarized in Table 2. Note that the colors in Table 2 match their corresponding datasets in Fig. 15 and Fig. 16 for easier reference. As can be seen in Fig. 15 and Fig. 16, at lower flap deflections, there was better agreement between the flight data and CFD data. Also, from Fig. 16, it can be observed that for flap deflections less than 15 deg as one moves away from the fuselage, C_l increased.

Table 2. Freestream conditions and airplane gross weight corresponding to Figs. 14 and 15.

Flap	Mach	Altitude, ft	Alpha, deg	Dynamic pressure, psf	Gross weight, lb
-2	0.304	9931	6.3	94	49830
0	0.294	9941	6.9	88	53960
2	0.297	9954	6.4	90	52910
5	0.301	9950	5.5	92	52650
10	0.299	9874	4.5	91	52090
15	0.296	9943	4.0	90	52170
20	0.298	9994	2.8	91	49330
25	0.304	9997	2.6	94	50830
30	0.302	9993	2.2	93	50470
-2	0.731	39880	3.3	147	50870
0	0.748	39850	2.7	155	50990
2	0.745	39880	2.5	153	53950
5	0.745	39970	1.8	152	51640
-2	0.554	20000	2.0	209	46020
0	0.535	19900	2.4	196	52360
5	0.550	20100	1.1	205	47730
10	0.542	20030	0.2	200	47100
15	0.543	20070	-0.5	200	45990

C. Stagnation Point Estimation

The leading edge stagnation point sensor was intended to track the stagnation point at all flight conditions. In initial low-altitude flight tests of less than 500 ft above ground level, the system functioned nominally; however, the ground temperature calibration proved insufficient for the colder temperatures at higher altitudes. Individual elements worked as expected, but collectively the system did not work as expected. However, an algorithm was developed that could track the stagnation point during maneuvers.

The algorithm was based on the supposition that a power decrease followed by an increase would indicate the stagnation point may have just moved across the sensor element. If this pattern is repeated across neighboring sensors, with the minimum power consumption shifting in time, it is very probable that the stagnation point had moved across the set of sensors. The algorithm was further updated to handle failed sensors as flights progressed, and the fine traces on the wiring became damaged. Overall, the leading edge stagnation point sensor was able to track a moving stagnation point during pitch maneuvers at a constant airspeed and altitude throughout the flight phases. A representative result of the processing algorithm is given in Fig. 17. Figure 17 shows the calculated stagnation point location for Mach 0.3 at 10,000 ft MSL. through three consecutive pitch maneuvers as a function of angle of attack. The vertical axis is distance from the leading edge, with positive values along the upper surface. The plot shows the most probable stagnation point based on filtered and unfiltered results of the algorithm. Since the sensor array consists of discrete sensors, the predicted stagnation point has discrete locations. Since the actual stagnation point is not subject to such constraints, the estimated stagnation point is filtered to allow the results to follow realistic behavior. For the clean wing (flaps 0 deg) flight condition, illustrated in Fig. 17, the stagnation point location agrees well with preflight CFD predictions.

D. Air Data

During baseline flights with the GIII airplane, the pitot-static system was characterized, and calibration curves, along with associated uncertainties, were created. The effects of the Fowler flap system on the pitot-static system were also characterized. Figure 18 shows the additional Mach correction curves necessary to correct for deployed Fowler flaps. Data were collected to evaluate any possible effects of the ACTE flap on the airplane pitot-static system. Analysis indicated that there was no discernable trend with respect to ACTE flap deflection. Mach calibration data for a subset of ACTE flap deflections are shown along with the Mach correction curves for the Fowler flaps in Fig. 19. Figure 20 shows results from an analysis of all pitot-static calibration data from the ACTE flights. These results indicate that, even when accounting for data scatter, any potential effects of the ACTE flaps fall within the uncertainty bounds of the baseline GIII airplane and do not show any consistent trend with increasing flap deflection.

VI. Conclusion

Compliant flaps, known as the ACTE flaps, were integrated onto a modified GIII airplane in support of the NASA Environmentally Responsible Aviation project as part of a joint effort with the AFRL. Prior to flight, analyses were performed to assess the aerodynamic effects of the ACTE flaps on the GIII airplane. The GIII airplane and the ACTE flaps were thoroughly instrumented to capture aerodynamic data during the planned flights. The modified airplane completed a series of flights with these flaps installed, with flap deflections ranging from -2 deg to 30 deg. During these flights, substantial aerodynamic data were collected and analyzed to evaluate the actual aerodynamic effects of the ACTE flap on the GIII airplane and compare these results with predictions.

Through the flight tests at all ACTE flap deflections, no major unexpected aerodynamic effects were noted due to the ACTE flaps. The primary effects of the flap on the airplane were as expected, added lift and pitching moment that increased with flap deflection along with a corresponding decrease in lift and pitching moment for the negative flap deflection, but the effects were not as strong as predicted for larger flap deflections. At ACTE flap deflections of 15 deg and larger, there was notable flow separation. Also, despite the fact that the baseline GIII Fowler flaps affected the pitot-static system, the ACTE flaps had no notable effects on the GIII system. The leading edge stagnation system did not work as initially anticipated, but was successfully used to track leading-edge stagnation point during a subset of flight-test maneuvers.

When comparing the aerodynamic flight-test results with predictions, it was found that modeling efforts over-predicted the change in lift and pitching moment due to the ACTE flap, corresponding with CFD solutions under-predicting flow separation and over-predicting suction prior to flow separation over the flap at larger deflections. The mismatch seen between the aerodynamic model and flight data is consistent with the local flow mismatches found between CFD and flight. These mis-predictions resulted in the airplane trimming at a higher-than-expected angle of attack, but due to added uncertainties and conservative flight guidelines, the difference in predicted and actual trim angle of attack was never problematic during flight testing.

In conclusion, the ACTE flaps were successfully flown on the NASA SCRAT airplane. The ACTE flaps generally affected the airplane as expected, but prediction methods over-predicted the effectiveness of the flaps at large deflections.

References

[1]Bui, T. T., "Analysis of Low-Speed Stall Aerodynamics of a Swept Wing with Seamless Flaps," AIAA 2016-####, 2016.

[2]Baumann, E., Hernandez, J., and Ruhf, J. C., "An Overview of NASA's SubsoniC Research Aircraft Testbed (SCRAT)," NASA TM-2013-216595, 2013.

[3]Miller, E. J., Cruz, J., Lung ,S.-F., Kota, S. Ph.D., Ervin, G., and Lu, K.-J. Ph.D., "Evaluation of the Hinge Moment and Normal Force Aerodynamic Loads from a Seamless Adaptive Compliant Trailing Edge Flap in Flight," AIAA 2016-0038, 2016.

[4]Herrera, C. Y., Spivey, N. D., and Lung, S.-F., "Aeroelastic Response of the Adaptive Compliant Trailing Edge Transition Section," AIAA 2016-0467, 2016.

[5]Smith, M. S., Bui, T. T., Garcia, C. A., and Cumming, S. B., "Longitudinal Aerodynamic Modeling of the Adaptive Compliant Trailing Edge Flaps on a GIII Airplane and Comparisons to Flight Data," AIAA 2016-####, 2016.

[6]Morelli, E. A., "Practical Aspects of the Equation-Error Method for Parameter Estimation," AIAA 2006-6144, 2006.

[7]Maine, R. E., and Iliff, K. W., "Application of Parameter Estimation to Aircraft Stability and Control, *The Output–Error Appr*oach," NASA RP-1168, 1986.

[8]Coleman, H. W., and Steele, W. G., "Experimentation and Uncertainty Analysis for Engineers," John Wiley & Sons, New York, 1999.

[9]Tao Systems, Senflex® Multi-Element Surface Hot-Film Sensors, URL: http://www.taosystem.com/products/senflex/ [cited 10, May 2016].

[10]Haering, E. A., Jr., "Airdata Calibration of a High-Performance Aircraft for Measuring Atmospheric Wind Profiles," NASA/TM-101714, 1990.

Figures

Figure 1. SCRAT airplane in flight with ACTE flaps installed (NASA ED15-076-26).

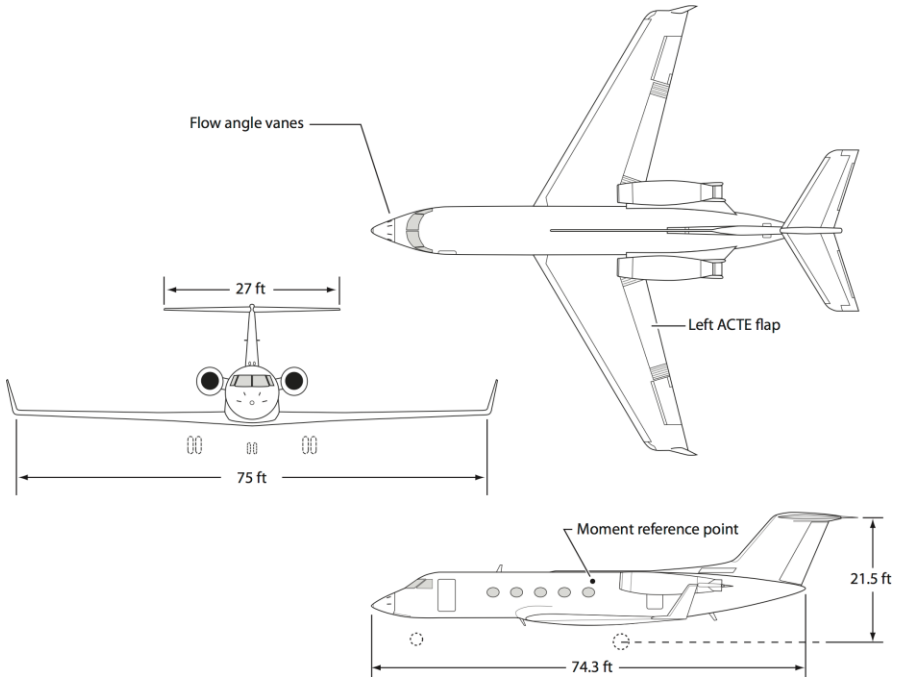

Figure 2. Three-view drawing of the GIII airplane.

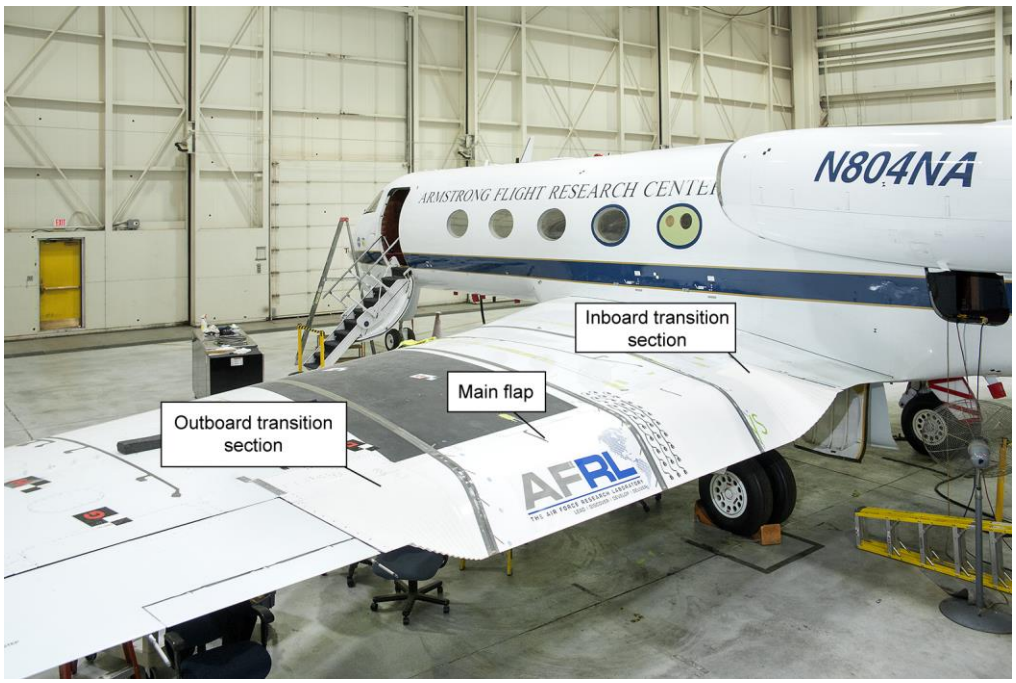

Figure 3. ACTE flap.

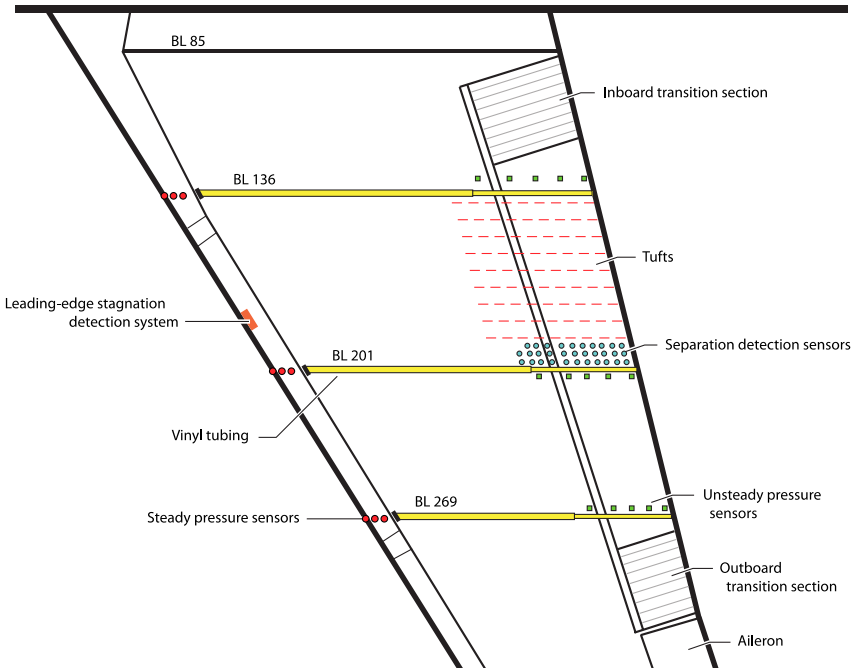

Figure 4. Illustrating top view of the left wing aerodynamic instrumentation.

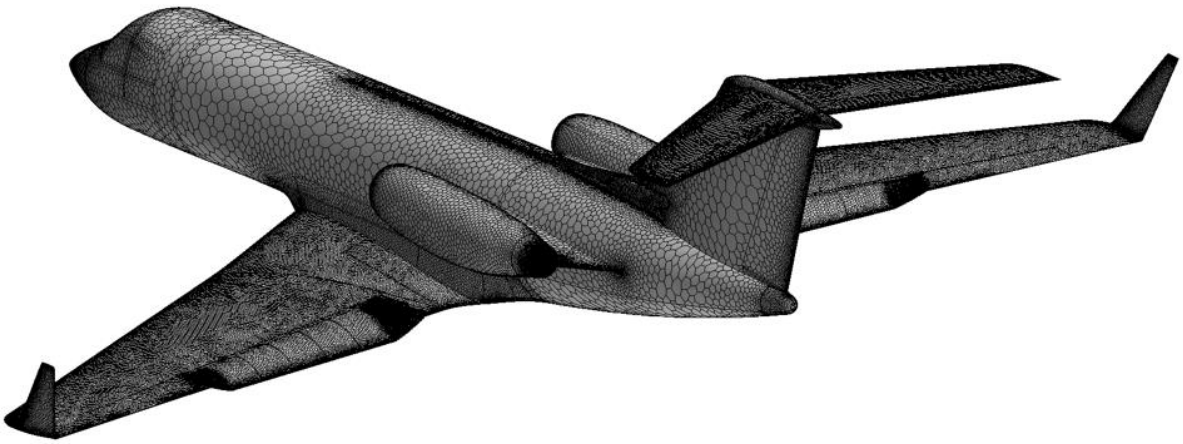

Figure 5. View of the STAR-CCM+ CFD surface mesh.

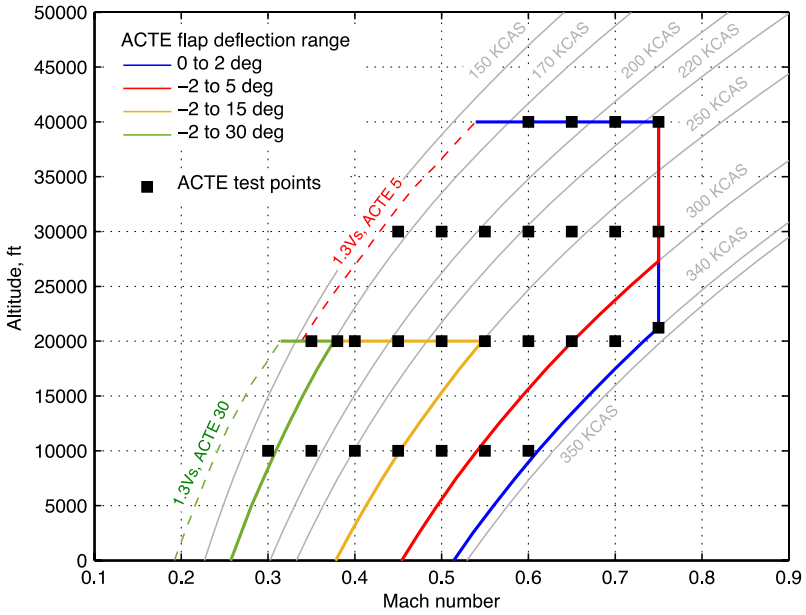

Figure 6. ACTE flight envelope.

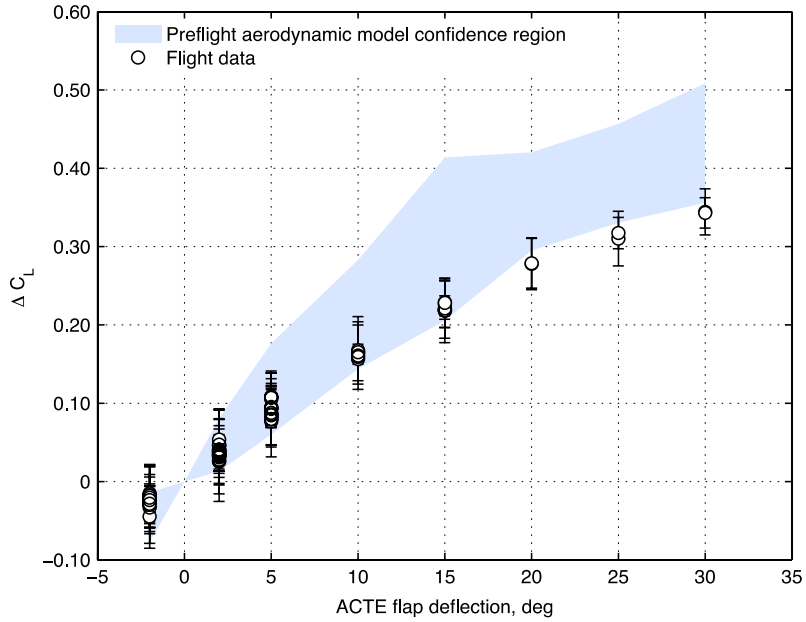

Figure 7. Predicted and in-flight estimated change in lift coefficients versus ACTE deflection.

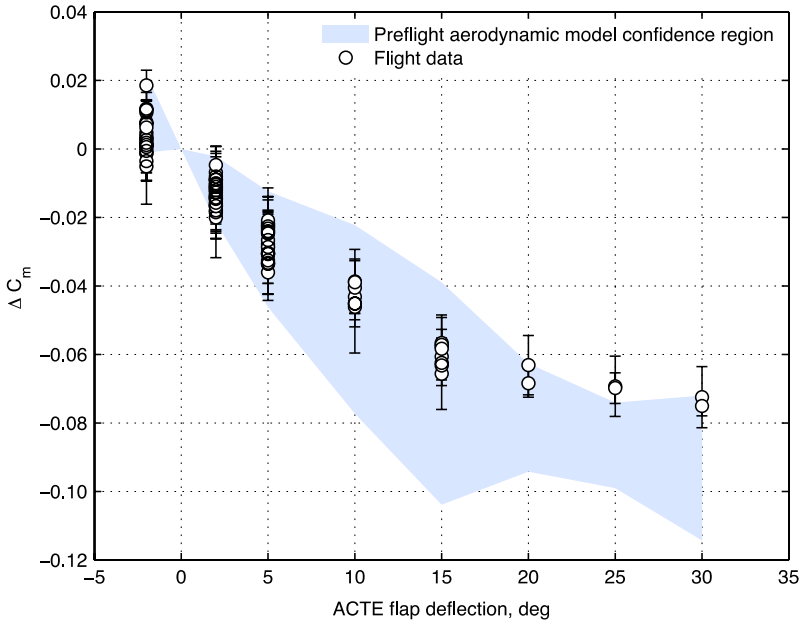

Figure 8. Predicted and in-flight estimated change in pitching moment coefficients versus ACTE deflection.

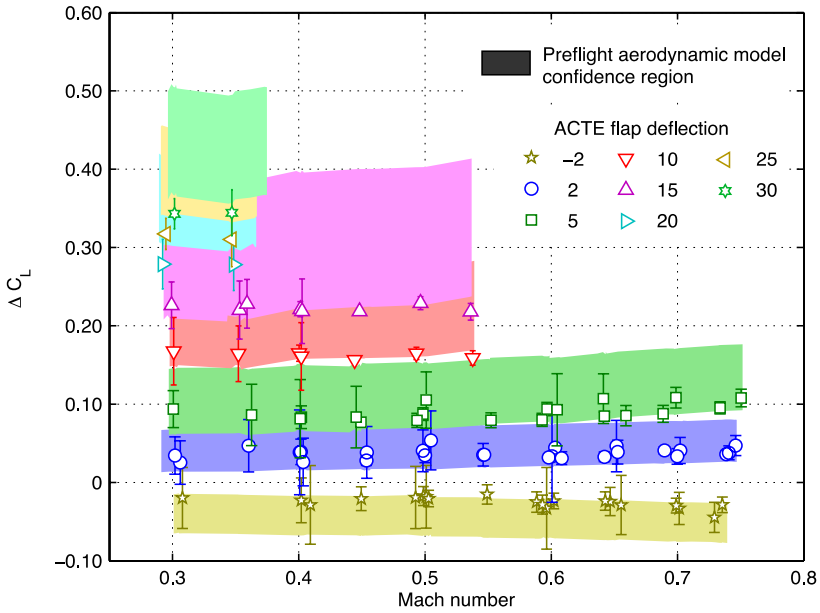

Figure 9. Predicted and in-flight estimated change in lift coefficients versus Mach number.

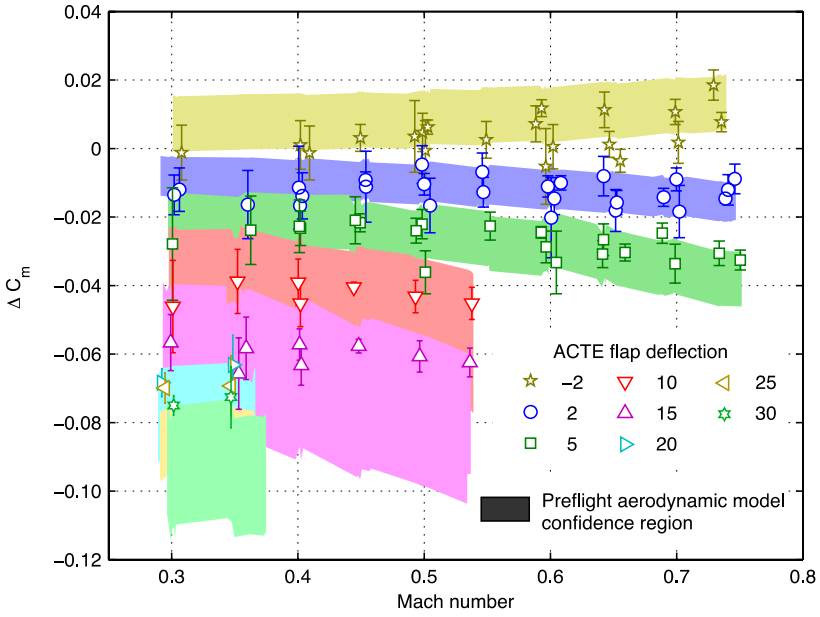

Figure 10. Predicted and in-flight estimated change in pitching moment coefficients versus Mach number.

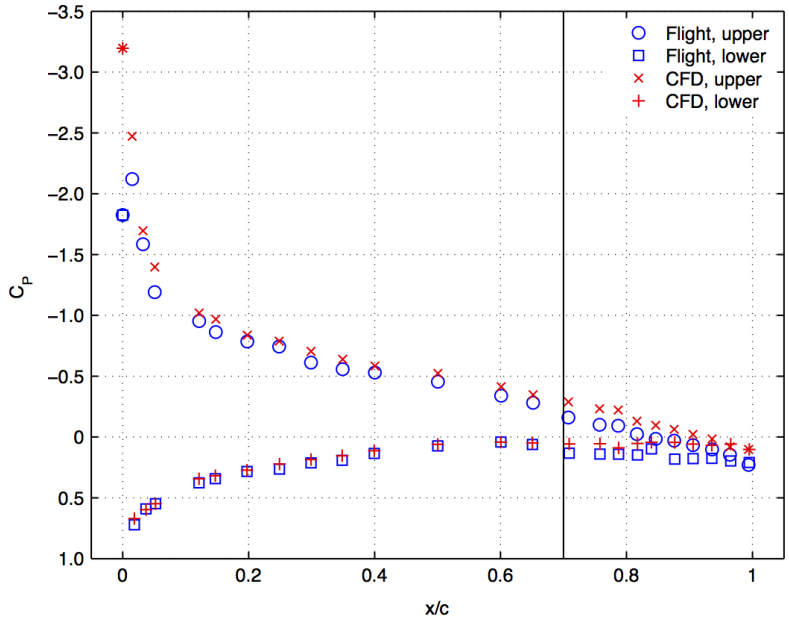

Figure 11. Pressure coefficient profile at the center butt line for Mach 0.30 at 10,000 ft MSL with an ACTE deflection of 0 deg.

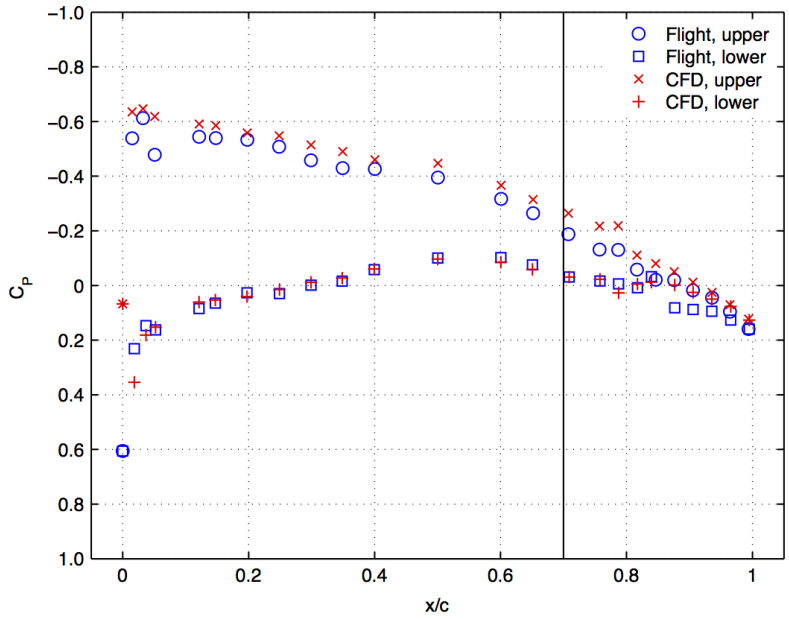

Figure 12. Pressure coefficient profile at the center butt line for Mach 0.55 at 20,000 ft MSL with an ACTE deflection of 0 deg.

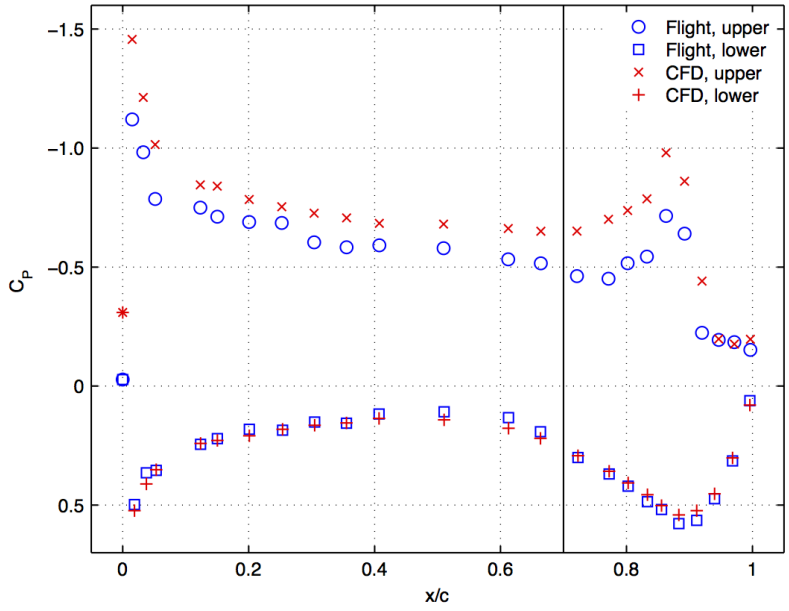

Figure 13. Pressure coefficient profile at the center butt line for Mach 0.30 at 10,000 ft MSL with an ACTE deflection of 20 deg.

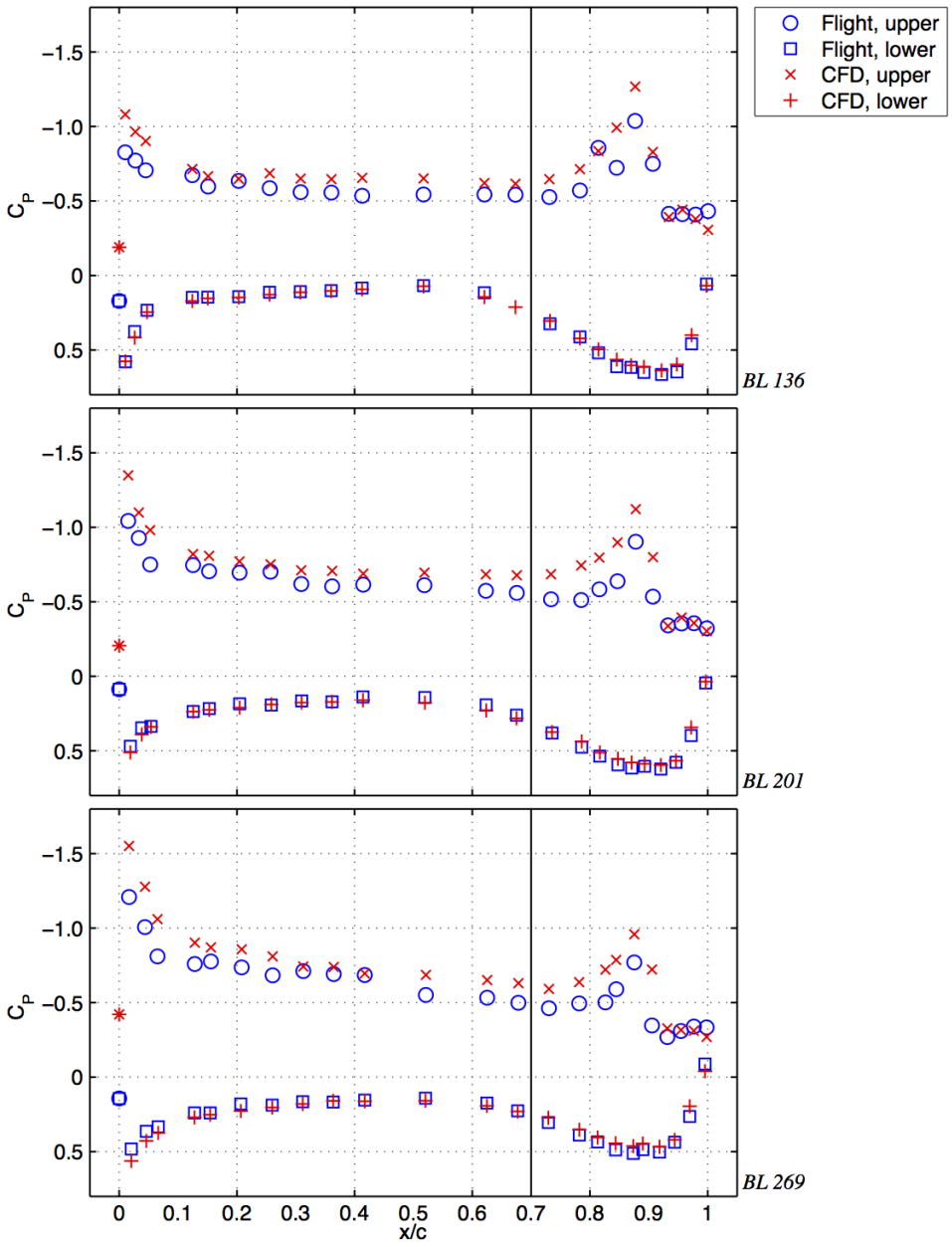

Figure 14. Pressure coefficient profiles for Mach 0.30 at 10,000 ft MSL with an ACTE deflection of 30 deg.

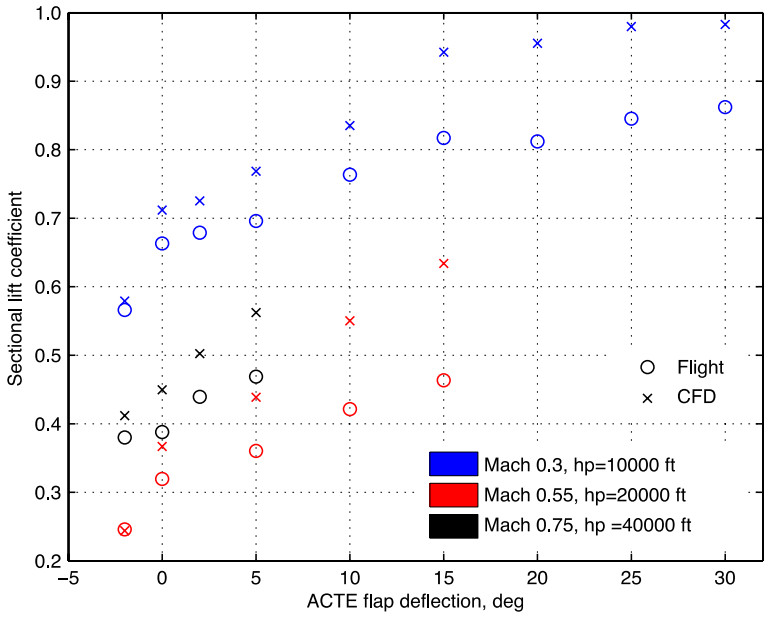

Figure 15. Trends in sectional lift at butt line 201.

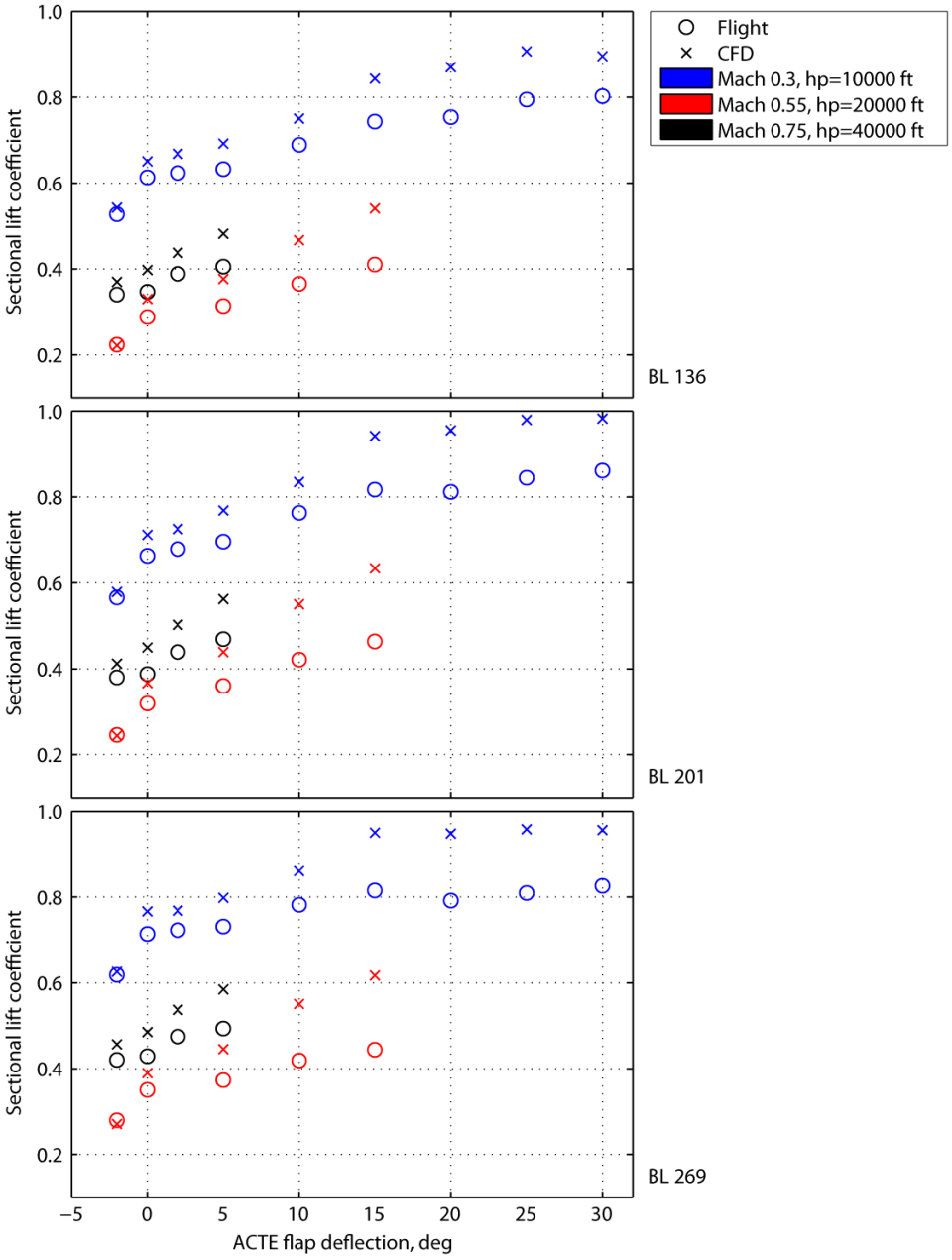

Figure 16. Trends in sectional lift at all three instrumented butt lines.

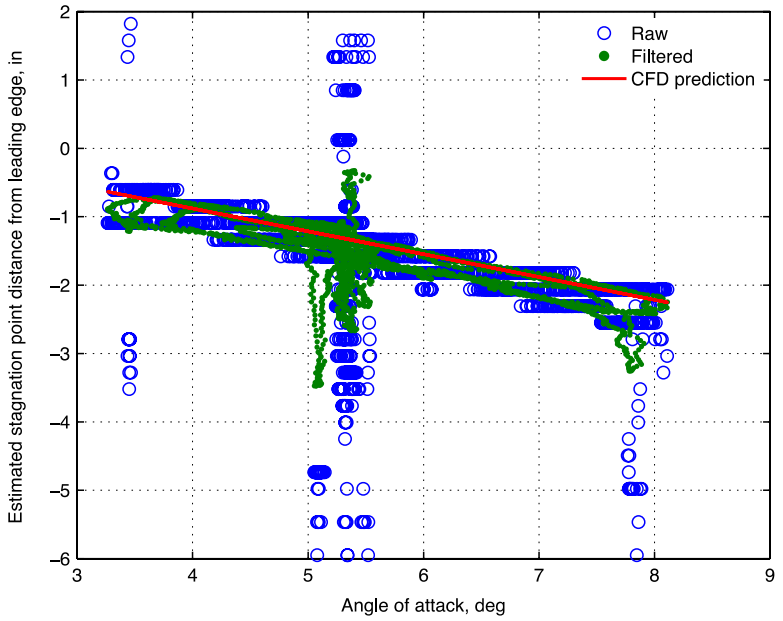

Figure 17. Calculated stagnation point location for Mach 0.3 at 10,000 ft MSL at a 0-deg ACTE flap deflection through three consecutive pitch 2-1-1 maneuvers as a function of angle of attack.

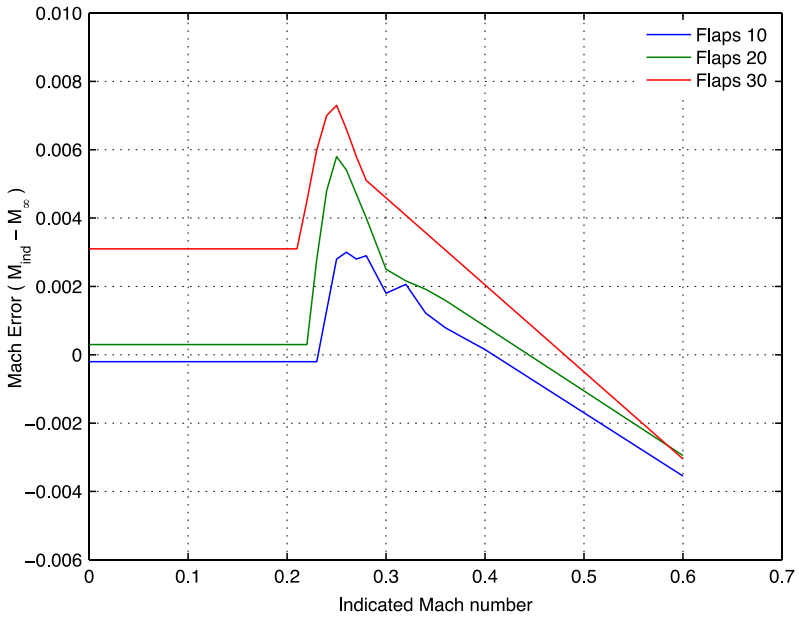

Figure 18. Additional Mach correction curves for the Fowler flaps.

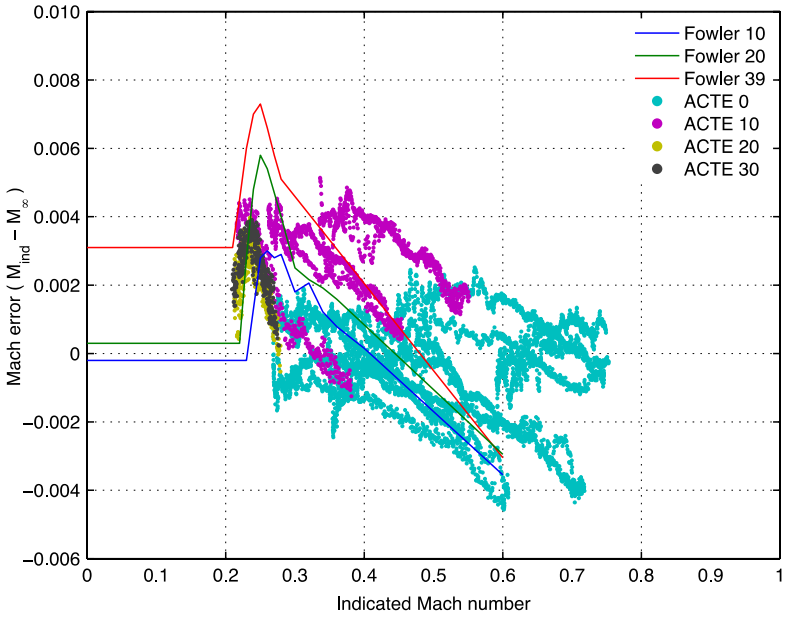

Figure 19. Fowler flap Mach correction curves and ACTE Mach correction flight data.

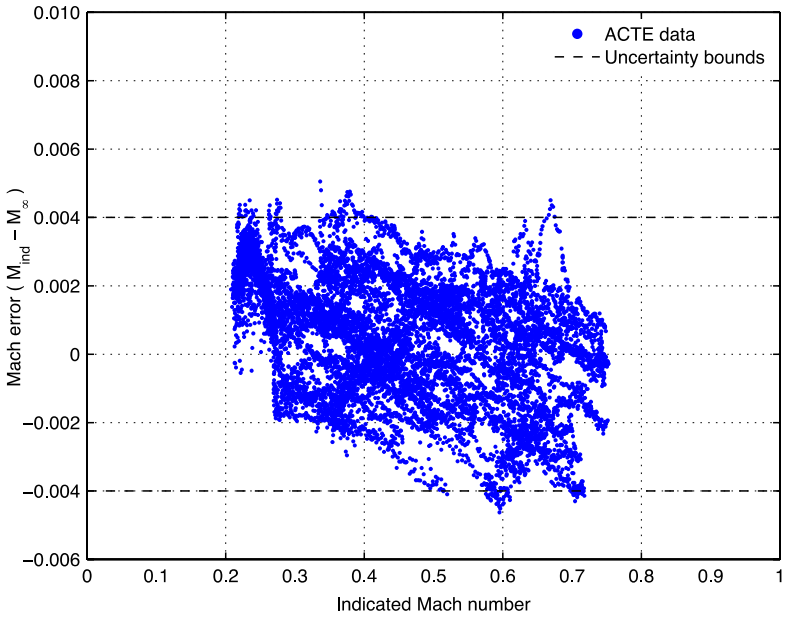

Figure 20. All ACTE Mach correction data with baseline calibration uncertainties.